Local Atomic Arrangement and Electronic Structure of Nanocrystalline Transition Metal Oxides Determined by X-ray Absorption Spectroscopy

Seong-Ju Hwang*,† and Jin-Ho Choy‡

Department of Applied Chemistry, College of Natural Sciences, Konkuk University Chungju Campus, Chungju, Chungbuk 380-701, Korea, and National Nanohybrid Materials Laboratory, School of Chemistry, Seoul National University, Seoul 151-747, Korea

Received: January 9, 2003; In Final Form: March 24, 2003

The local crystal structure and electronic configuration of transition metal in X-ray amorphous MnO_2 and CrO_2 nanocrystals have been examined by using X-ray absorption (XAS) spectroscopy at Mn K and Cr K-edges. The Mn K-edge XAS study reveals that tetravalent manganese ions are stabilized in α-MnO_2-type local atomic arrangement consisting of the intergrowth of edge- and corner-shared MnO_6 octahedra. On the other hand, it is found from Cr K-edge XAS results that nanocrystalline CrO_2 possesses two different kinds of local structures around chromium, that is, Cr_2O_3-type with octahedral site and CrO_3-type with tetrahedral site. The presence of Cr^{+VI} species on the surface would be helpful for Li grafting process, giving rise to excellent electrochemical performances. This work can be regarded as a strong evidence for the usefulness of XAS to study nanocrystalline electrode materials.

Introduction

Recently intense research interest has been focused on the nanocrystalline transition metal oxides as promising electrode materials for lithium rechargeable batteries.[1−5] One of the main advantages of nanocrystalline materials is their high structural stability for repeated Li insertion−disinsertion processes, leading to an improved cyclability and a great discharge capacity. This is surely contrasted with well-crystalline materials that frequently suffer from severe phase transition upon the Li intercalation−disintercalation process.[6,7] Until now, several nanocrystalline metal oxides have been explored as an alternative electrode material.[1−5,8,9] Among them, nanocrystalline 3d transition metal oxides such as MnO_2 and CrO_2 have attracted special attention due to their lightweight and high energy density.[3−5,8] However, there have been only a few studies dealing with their crystal and electronic structures.[10,11] This would be because this kind of nanocrystalline material prepared by *Chimie Douce* reaction at low temperature is often X-ray amorphous because of the lack of long range crystal order. For this reason, X-ray diffraction (XRD), which is a common tool for structure analysis of inorganic solids, is not suitable for studying these nanocrystalline materials. It is therefore required to employ other spectroscopic methods to investigate the local chemical environment and, at the same time, the chemical bonding nature of a nanocrystalline electrode. Actually, we have demonstrated that X-ray absorption spectroscopy (XAS) is very effective in probing the local atomic structure of electrode materials with poor crystallinity, as well as in examining the effect of the Li insertion−disinsertion process on it.[7,12] Moreover, XAS can provide electronic structural information on a specific absorbing atom from X-ray absorption near-edge structure (XANES) data, as well as local structural information on the neighboring atoms of an absorber through extended X-ray absorption fine structure (EXAFS) analysis.[13]

In this study, we have applied XAS to the study on the chemical bonding nature of nanocrystalline MnO_2 and CrO_2 compounds prepared by reduction of $KMnO_4$ and K_2CrO_4 at room temperature. Even though there are many structure types for MnO_2, the present XANES/EXAFS results allow us to identify the exact local structure of nanocrystalline MnO_2. In the case of CrO_2 nanocrystal, however, two different local crystal structures corresponding to Cr_2O_3- and CrO_3-types could be observed.

Experimental Section

The nanocrystalline MnO_2 and CrO_2 samples were prepared by reacting the aqueous solution of $KMnO_4$ or K_2CrO_4 with KBH_4 at room temperature, as previously reported.[4a,8] Briefly, MnO_2 nanocrystals were obtained by dropwise addition of 50 mL of 0.1 M KBH_4 solution to 50 mL of 0.1 M $KMnO_4$ solution at pH 1, and CrO_2 sample was prepared by dropwise addition of 50 mL of 0.1 M KBH_4 solution to 50 mL of 0.25 M K_2CrO_4 solution at pH 2. During the titration process, concentrated HCl was added to maintain constant pH condition because pH tends to increase due to the formation of KOH and KBO_2. Nanocrystals were washed thoroughly with distilled water and dried at 110 °C under vacuum. The effect of heat treatment on the crystal structures of nanocrystalline MnO_2 and CrO_2 compounds was studied by XRD measurements using Ni-filtered Cu Kα radiation with a graphite diffracted beam monochromator. The chemical composition of these nanocrystals was examined by using energy dispersive spectrometric (EDS) analysis, which confirmed the absence of potassium ion and the formation of binary oxides. As a reference material for XAS measurements, nanocrystalline K−Li−Mn−O−I was prepared by mixing the aqueous solution of $KMnO_4$ with 1.5 equiv of LiI at room temperature,[10] and the spinel $LiMn_{1.8}Cr_{0.2}O_4$ was synthesized by conventional solid-state reaction with the stoichiometric mixture of $LiCO_3$, Mn_2O_3, and Cr_2O_3 precursors.[12c]

* To whom correspondence should be addressed. Tel: +82-43-840-3569. Fax: +82-43-851-4169. E-mail: hwangsju@kku.ac.kr.
† Konkuk University Chungju Campus.
‡ Seoul National University.

10.1021/jp034049d CCC: $25.00
Published on Web 05/24/2003

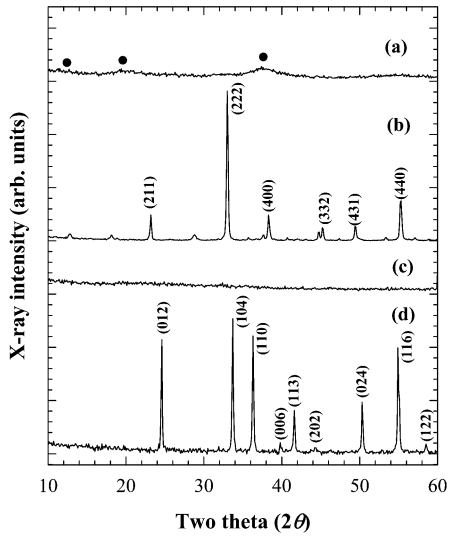

Figure 1. Powder XRD patterns of (a) nanocrystalline MnO_2 compound and (b) its derivative after the heat treatment at 600 °C, together with (c−d) the corresponding data of CrO_2 compound. In panels b and d, the indexed reflections originate from Mn_2O_3 and Cr_2O_3, respectively.

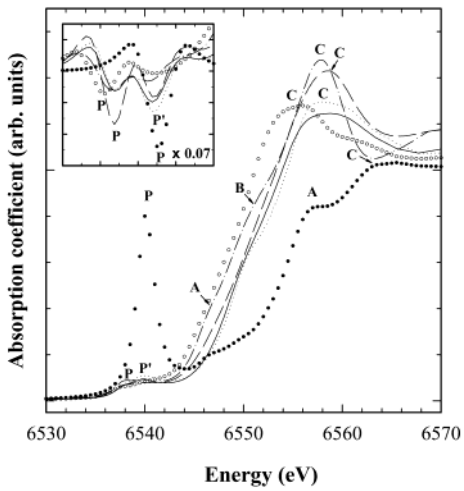

Figure 2. Mn K-edge XANES spectrum for the nanocrystalline MnO_2 compound (—), in comparison with those for the references Mn_2O_3 (○), nanocrystalline K−Li−Mn−O−I (− − −), spinel $LiMn_{1.8}Cr_{0.2}O_4$ (− · −), β-MnO_2 (···), and $KMnO_4$ (●). The inset presents corresponding second derivative spectra for preedge region of 6535−6543 eV. In the inset, data of $KMnO_4$ are multiplied by 0.07 because of their great amplitude.

The XAS experiments on the nanocrystalline MnO_2 and CrO_2 compounds and some references were performed with the EXAFS facility installed at the beam line 7C at the Photon Factory in Tsukuba.[14] The XAS data were collected at room temperature in a transmission mode using gas-ionization detectors. All of the present spectra were calibrated by measuring the spectra of Mn and Cr metal foils. The data analysis for the experimental spectra was carried out by the standard procedure as reported previously.[13] We have constructed a variety of structure models by adopting the crystallographic structure data of manganese oxides and chromium oxides, such as α-MnO_2, β-MnO_2, γ-MnO_2, CrO_2, Cr_2O_3, and CrO_3, for quantitative EXAFS analysis.[15−20]

Results and Discussion

Figure 1 represents the powder XRD patterns of MnO_2 and CrO_2 compounds before and after heat treatment at 600 °C. Well-defined reflection was not observed for both samples, indicating their nanocrystalline nature. Unlike CrO_2 nanocrystal, MnO_2 shows several very broad and diffuse features at around 12°, 19°, and 38°, indicating that the structural coherence unit is longer for MnO_2 than for CrO_2. No change was observed in XRD patterns before and after heating at 110 °C under vacuum. In contrast, the heat treatment at 600 °C in air gives rise to a crystallization of amorphous phase to M_2O_3 (M = Mn and Cr) phase, together with a loss of 0.5 oxygen per transition metal. As mentioned above, X-ray amorphous character of the as-prepared nanocrystals makes XRD useless in the determination of their crystal structures. In this regard, we have applied XAS not only to identify the local crystal structure but also to probe the electronic structure of these materials.

The Mn K-edge XANES spectrum of nanocrystalline MnO_2 is presented in Figure 2, in comparison with the reference spectra of nanocrystalline manganese oxyiodide K−Li−Mn−O−I, cubic spinel $LiMn_{1.8}Cr_{0.2}O_4$, Mn_2O_3 (bixbyite), β-MnO_2 (pyrolusite), and $KMnO_4$. The position of edge jump for the nanocrystalline MnO_2 is nearly the same as that for the reference β-MnO_2 but slightly higher than those for nanocrystalline manganese oxyiodide and $LiMn_{1.8}Cr_{0.2}O_4$. This indicates that manganese ions in MnO_2 nanocrystal have an average valence state of ∼4, which is well consistent with the previous results on the chemical analysis.[21] In the preedge region, all of the spectra presented here show small preedge peaks (denoted P and P′), which are assigned as the transitions from the core 1s level to unoccupied 3d states. Even though they are not allowed by the electronic dipolar selection rule, $\Delta l = \pm 1$, the preedge peaks can be discerned either because of quadrupole-allowed transitions or because of the mixing of 4p and 3d states or both.[22] Therefore, this feature obtains significant spectral weight for the case of noncentrosymmetric local geometry of an absorbing atom. In fact, a very intense feature P is detected for the reference $KMnO_4$ with the tetrahedral Mn^{+VII} ion. In contrast, the weak intensity of the preedge peak for nanocrystalline MnO_2 suggests that the manganese ions are stabilized in octahedral site with an inversion center, as in Mn_2O_3, spinel $LiMn_{1.8}Cr_{0.2}O_4$, and β-MnO_2. The position and shape of these preedge peaks are closely related to the oxidation state of the absorbing ion and the local arrangement of backscattering ions, respectively.[10,13] As can be seen clearly from the inset of Figure 2, the relative energies of these peaks are consistent with the order of the main edge positions. It is also evident that the spectral shape of preedge features is strongly dependent upon Mn oxidation state; one feature P at 6537 eV is observed for Mn_2O_3 containing trivalent manganese ions only, whereas two preedge peaks P and P′ are discernible for other materials containing a considerable amount of tetravalent manganese ions. A closer inspection reveals that Mn oxidation state also has influence on the intensity ratio of the two preedge peaks P and P′. That is, while the peak P′ is more intense than the peak P for both nanocrystalline and reference MnO_2 compounds, a reversal of relative intensity is detected for $LiMn_{1.8}Cr_{0.2}O_4$ and K−Li−Mn−O−I with mixed Mn^{+III}/Mn^{+IV} oxidation state. This confirms that the average oxidation state of manganese ion in nanocrystalline MnO_2 is tetravalent as in β-MnO_2. In the main-edge region, there are some peaks (denoted A, B, and C) that are assigned as the dipole-allowed transitions from the core 1s level to unoccupied 4p states. Among these features, the peak C should be carefully noted because it can provide useful information on the crystal framework of manganese oxide.[10] As shown in Figure 2, the nanocrystalline MnO_2 and reference β-MnO_2 show a weak and broad peak C, whereas an intense and sharp peak C appears for the spinel lithium manganate and

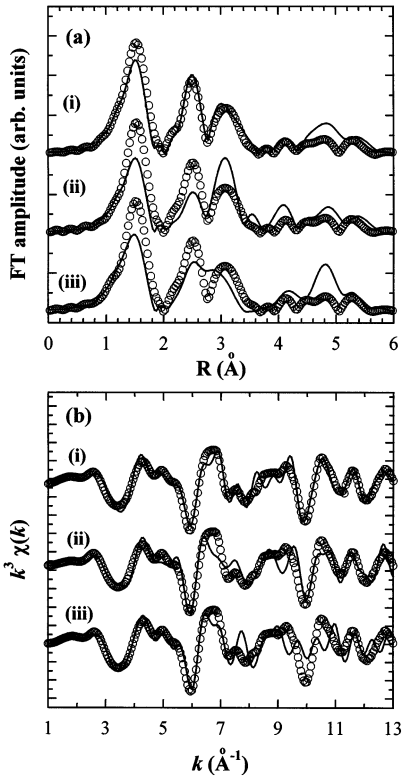

Figure 3. Experimental Mn K-edge EXAFS spectra (○) in (a) *R*- and (b) *k*-space, in comparison with the simulated spectra (—) based on the structure of (i) α-MnO_2, (ii) *β*-MnO_2, and (iii) *γ*-MnO_2.

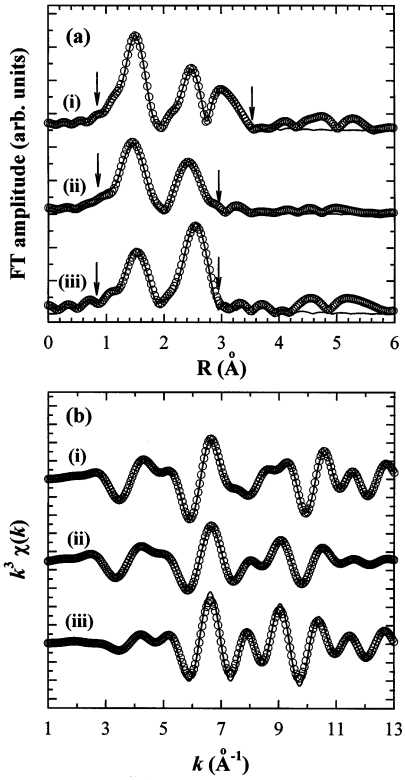

Figure 4. Fourier (a) transformed and (b) filtered Mn K-edge EXAFS spectra for (i) nanocrystalline MnO_2, (ii) nanocrystalline K−Li−Mn−O−I, and (iii) spinel $LiMn_{1.8}Cr_{0.2}O_4$. The range over which the Fourier filtering has been made is shown by the arrows. The solid lines and empty circles represent the fitted and experimental data, respectively.

nanocrystalline manganese oxyiodide. Considering the fact that the intensity of this peak is proportional to the relative concentration of edge-shared MnO_6 octahedra with respect to corner-shared one,[23] it can be supposed that the crystal structure of nanocrystalline MnO_2 contains corner-shared MnO_6 octahedra in significant concentration. In contrast, the observed sharp peak C in $LiMn_{1.8}Cr_{0.2}O_4$ and K−Li−Mn−O−I clarifies that there are only edge-shared MnO_6 octahedra, which is in good agreement with their crystal structures, that is, spinel- and layered-type.[10,12c] From the present XANES results, we are able to obtain a measure for identifying the local structure of nanocrystalline manganese oxide. Among various crystal structures of MnO_2 such as α-, *β*-, *γ*-, *ϵ*-, and *λ*-form (spinel-type) and layered phase, the latter three structures consisting of the network of edge-shared MnO_6 octahedra[16,24] cannot be adopted as a local structure of nanocrystalline MnO_2 because the weak and broad peak C underlines the presence of corner-shared MnO_6 octahedra. Therefore, the remaining candidates are α-, *β*-, and *γ*-MnO_2-type structure.[16,17] However, on the basis of the present XANES results, we were unable to evaluate the validity of these models. To solve this problem, we have performed EXAFS fitting analyses with these structures.

For the purpose of evaluating the validity of these structural models, first we have simulated theoretically the EXAFS data on the basis of α-, *β*-, and *γ*-MnO_2 structures. The experimental and simulated spectra in *R*- and *k*-space are shown in panels a and b, respectively, of Figure 3. In Fourier transform (FT) diagram (Figure 3a), the first peak at ∼1.5 Å corresponds to (Mn−O) bonding pair, whereas the following peaks at ∼2.5 and ∼3.1 Å originate from (Mn−Mn) shells in the edge- and corner-shared MnO_6 octahedra pairs, respectively. The main difference among the three structural models is the relative concentration of corner-sharing to edge-sharing of MnO_6 octahedra. As can be seen clearly from Figure 3a, the α-MnO_2 structure allows us to reproduce well two FT peaks corresponding to (Mn−Mn) shells. The best consistency in *k*-space data was also obtained with α-MnO_2 structure (Figure 3b). This observation can be regarded as a strong evidence for α-MnO_2-type local structure in nanocrystalline MnO_2. In fact, α-MnO_2 structure having large 2 × 2 pores is most favorable for the repeated Li insertion−disinsertion.[15] To determine the structural parameters such as coordination number (CN), bond distance (*R*), and Debye−Waller factor (σ^2), these FT peaks were isolated by inverse FT to a *k* space and then curve-fitted.[25] The experimental and fitted FT and inverse FT spectra of nanocrystalline MnO_2 are represented in panels a and b of Figure 4, respectively, in comparison with those of nanocrystalline K−Li−Mn−O−I and spinel $LiMn_{1.8}Cr_{0.2}O_4$ and the curve-fitting results are collected in Table 1. On the basis of α-MnO_2 structure, a good fit was obtained for nanocrystalline MnO_2 in the *R*-range up to 3.6 Å. The best-fit bond distances of (Mn−O) and (Mn−Mn) shells are well consistent with the crystallographic values,[15] confirming the reliability of fitting analysis. In contrast to nanocrystalline MnO_2, no FT peak appears around 3 Å for nanocrystalline K−Li−Mn−O−I and spinel $LiMn_{1.8}Cr_{0.2}O_4$ because they do not have corner-shared MnO_6 octahedra. It should be noted here that the nanocrystalline K−Li−Mn−O−I crystallizes with rhombohedral layered structure,[10] which is dissimilar to the case of the present MnO_2 nanocrystal. Such a structural difference between both nanocrystalline compounds would be ascribed to the presence of potassium ion that can act as pillar species for stabilizing the layered structure. It is also worthwhile to mention that nanocrystalline MnO_2 shows small but distinct FT peaks in 4−6 Å region, which are absent in nanocrystalline K−Li−Mn−O−I. This implies that the structural coherence is greater for the former than for the latter, as

TABLE 1: Results of Nonlinear Least Square Curve Fittings for the Mn K-Edge EXAFS Spectra of Nanocrystalline MnO_2, K−Li−Mn−O−I, and Spinel $LiMn_{1.8}Cr_{0.2}O_4$

sample	bond	CN	R (Å)	σ^2 ($10^{-3} \times$ Å^2)
nanocrystalline	Mn−O[b]	2.0	1.89[c]	3.64
MnO_2[a]	Mn−O[b]	1.0	1.89[c]	3.64
	Mn−O[b]	1.0	1.90	3.64
	Mn−O[b]	2.0	1.91	3.64
	Mn−Mn[b]	2.0	2.85	5.78
	Mn−Mn[b]	2.0	2.89	5.78
	Mn−O[b]	1.0	3.39	2.86
	Mn−O[b]	1.0	3.41	2.86
	Mn−Mn[b]	4.0	3.42	5.12
	Mn−O[b]	2.0	3.42	2.86
	Mn−O[b]	2.0	3.43	2.86
	Mn−O[b]	1.0	3.54	2.86
nanocrystalline	Mn−O	6.0	1.90	4.89
K−Li−Mn−O−I	Mn−Mn	4.2	2.86	6.22
spinel	Mn−O	6.0	1.91	4.59
$LiMn_{1.8}Cr_{0.2}O_4$	Mn−Mn,Cr	6.0	2.90	4.29

[a] The curve fitting analysis was performed for the range of $0.859 \leq R \leq 3.59$ Å and $2.85 \leq k \leq 13.95$ Å^{-1}. [b] To avoid unnecessary computation, we have taken into account only single scattering (SS) paths for present fitting analysis. In fact, there is no multiple scattering (MS) path with focusing effect (i.e., bond angle of 180°), and hence, the contribution of any MS path is below 10% of the first shell maximum peak amplitude. [c] According to the crystallographic data of α-MnO_2, these bond distances are slightly different by 0.005 Å.

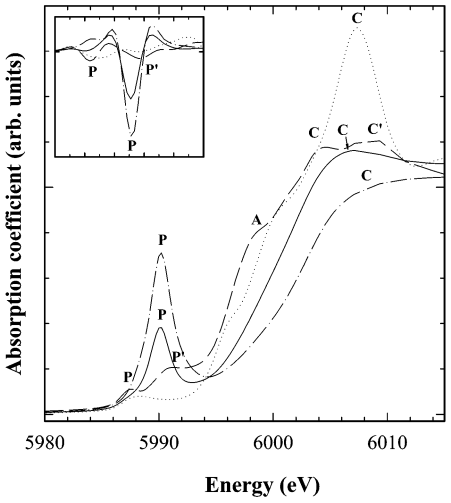

Figure 5. Cr K-edge XANES spectra for the nanocrystalline CrO_2 compound (—), in comparison with those for the references Cr_2O_3 (− − −), CrO_3 (−· −), and spinel $LiMn_{1.8}Cr_{0.2}O_4$ (···). The inset presents corresponding second derivative spectra for preedge region of 5985−5995 eV.

suggested from XRD analyses. These phenomena can be rationalized by taking into account their different synthetic methods in which the former was prepared by dropwise addition of KBH_4 solution to $KMnO_4$ solution, while the latter was obtained by rapid addition of LiI to $KMnO_4$ solution. The slower mixing of reactants gives rise to a more effective crystal growth of MnO_2 crystallites.

Figure 5 illustrates the Cr K-edge XANES spectrum of nanocrystalline CrO_2, together with those of the references Cr_2O_3, CrO_3, and spinel $LiMn_{1.8}Cr_{0.2}O_4$. The edge energy of nanocrystalline CrO_2 is lower than that of CrO_3 but higher than those of Cr_2O_3 and $LiMn_{1.8}Cr_{0.2}O_4$, highlighting the tetravalent oxidation state of chromium in this compound. In contrast to the reference CrO_3 with tetrahedral Cr^{+VI} ions,[20] the preedge peak P related to the dipole-forbidden 1s → 3d transition is

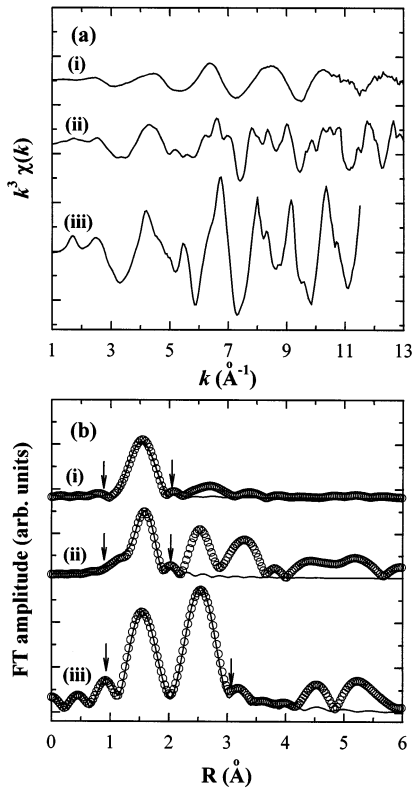

Figure 6. k^3-weighted Cr K-edge (a) EXAFS spectra and (b) their FTs for (i) the nanocrystalline CrO_2 compound, (ii) Cr_2O_3, and (iii) spinel $LiMn_{1.8}Cr_{0.2}O_4$. The range over which the Fourier filtering has been made is shown by the arrows. In panel b, the solid lines and empty circles represent the fitted and experimental data, respectively.

fairly weak in intensity for $LiMn_{1.8}Cr_{0.2}O_4$ and Cr_2O_3 with trivalent chromium ion in the octahedral site. In the case of nanocrystalline CrO_2, a rather intense peak P is also detected, suggesting the tetrahedral symmetry around chromium. This is inconsistent with the crystallographic data of crystalline CrO_2 in which Cr is stabilized in slightly distorted CrO_6 octahedra with the bond distances of 1.9006 (×4) and 1.9048 Å (×2).[18] In this regard, we have carried out Cr K-edge EXAFS analyses to exactly determine the local structure around chromium.

The k^3-weighted Cr K-edge EXAFS spectra for nanocrystalline CrO_2, reference Cr_2O_3, and spinel $LiMn_{1.8}Cr_{0.2}O_4$ are plotted in Figure 6a and the corresponding FTs in Figure 6b. The results of curve fitting are collected in Table 2. In contrast to Cr_2O_3 and spinel $LiMn_{1.8}Cr_{0.2}O_4$, CrO_2 shows no well-defined FT features except the first peak corresponding to (Cr−O) shell, evidencing its nanocrystalline character. We tried to fit the spectrum of nanocrystalline CrO_2 for the estimation of structural parameters. Unfortunately, the attempt based on the crystallographic structure data of CrO_2[18] failed. And other trials with Cr_2O_3 or CrO_3 structure[19,20] were also found to be unsuccessful. Alternatively, we constructed mixture models by combining the crystal structures of Cr_2O_3 and CrO_3, and by combining those of CrO_2 and CrO_3. As shown in Figures 6b and 7, an excellent fit could be obtained with a mixture model of Cr_2O_3 and CrO_3 structures,[27] clarifying that the chromium ions in nanocrystalline CrO_2 are located not only in tetrahedral site with the average (Cr−O) bond distance of 1.75 Å but also in octahedral site with the average (Cr−O) bond distance of 1.98 Å. The relative concentration of Cr_2O_3- and CrO_3-type structures was evaluated to be 0.56 and 0.44, respectively, with the average Cr oxidation state of 4.3. This is in good agreement with the edge position in XANES spectra. The other mixture

TABLE 2: Results of Nonlinear Least Square Curve Fittings for the Cr K-Edge EXAFS Spectra of Nanocrystalline CrO_2, Cr_2O_3, and Spinel $LiMn_{1.8}Cr_{0.2}O_4$

sample	bond	CN	R (Å)	σ^2 ($10^{-3} \times$ Å^2)
nanocrystalline CrO_2[a]	Cr−O[b]	1 × 0.44[d]	1.66[e]	1.93
	Cr−O[b]	1 × 0.44[d]	1.66[e]	1.93
	Cr−O[b]	2 × 0.44[d]	1.83	1.93
	Cr−O[c]	3 × 0.56[d]	1.93	1.28
	Cr−O[c]	3 × 0.56[d]	2.02	1.28
Cr_2O_3	Cr−O	3.0	1.94	1.14
	Cr−O	3.0	2.03	1.14
$LiMn_{1.8}Cr_{0.2}O_4$	Cr−O	6.0	1.98	2.58
	Cr−Mn,Cr	6.0	2.89	3.22

[a] The curve fitting analysis was performed for the range of $0.920 \leq R \leq 2.117$ Å and $3.75 \leq k \leq 13.5$ Å^{-1}. [b] These three shells originate from the Cr−O coordination sphere in CrO_3 phases. [c] These two shells originate from the Cr−O coordination sphere in Cr_2O_3 phases. [d] The present coordination numbers are multiplied by the relative concentration of Cr_2O_3 and CrO_3 phases. [e] According to the crystallographic data of CrO_3, these bond distances are slightly different by 0.004 Å.

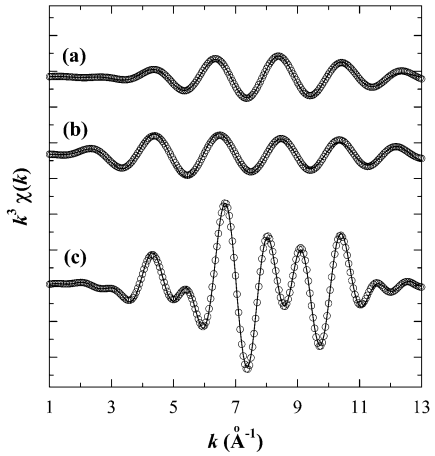

Figure 7. Fourier filtered Cr K-edge EXAFS spectrum for the (a) nanocrystalline CrO_2 compound, in comparison with those for the references (b) Cr_2O_3 and (c) spinel $LiMn_{1.8}Cr_{0.2}O_4$. The solid lines and empty circles represent the fitted and experimental data, respectively.

model of CrO_2 and CrO_3 structures also gave an acceptable fit, but the resulting (Cr−O) bond distances were determined to be 1.74 and 1.97 Å, which correspond to the bond distances of (Cr^{+VI}−O) and (Cr^{+III}−O), respectively.[19,20] This provides a clear evidence on the coexistence of trivalent and hexavalent chromium ions, as well as on the absence of tetravalent chromium ion. Judging from our previous report on nanocrystalline $LiMn_2O_4$ showing the Mn oxidation state is higher for the surface species,[1a] the hexavalent chromium ion would exist on the surface of particles while the trivalent chromium would be in the core of particles. This is further supported by the fact that an incomplete coordination for surface species would favor lower coordination number. As suggested from the "electrochemical grafting" concept,[1a,2b,28] the easily reducible Cr^{+VI} species on the surface are presumed to provide active sites for Li^+ grafting, leading to an improved electrochemical activity for this nanocrystalline CrO_2 compound. In fact, this material was known to exhibit better electrochemical performances compared to the well-crystalline CrO_2 compound.[8,29]

Conclusion

We have elucidated the electronic and crystal structures of X-ray amorphous MnO_2 and CrO_2 nanocrystals by applying XAS analysis. From the Mn K-edge XANES/EXAFS results, we have found that the tetravalent manganese ions are stabilized in octahedral sites with α-MnO_2-type local structure. The presence of large 2 × 2 pores in α-MnO_2-type structure would allow the present nanocrystalline MnO_2 to accommodate the lithium ion in a reversible way and to become a promising electrode material for lithium secondary battery. On the other hand, Cr K-edge XAS study reveals that there are two kinds of chromium ions in nanocrystalline CrO_2, a trivalent Cr ion in octahedral symmetry with Cr_2O_3-type local structure and a hexavalent Cr ion in a tetrahedral site with CrO_3-type local structure. The latter species is presumed to exist on the surface of particles, resulting in an easy grafting process of lithium ion and an improved electrochemical activity. The present work demonstrates that XANES/EXAFS is a very powerful tool not only for determining the local crystal and electronic structures of nanocrystalline materials but also for understanding their physicochemical properties.

Acknowledgment. This work was supported by the Faculty Research Fund of Konkuk University in 2002 and in part by the Korean Ministry of Science and Technology through the NRL project '99. Authors are also grateful to Prof. M. Nomura for helping us to get the XAS data in the Photon Factory.

References and Notes

(1) (a) Treuil, N.; Labrugère, C.; Menetrier, M.; Portier, J.; Campet, G.; Deshayes, A.; Frison, J. C.; Hwang, S. J.; Song, S. W.; Choy, J. H. *J. Phys. Chem. B* **1999**, *103*, 2100. (b) Kang, S. H.; Goodenough, J. B.; Rabenberg, L. K. *Electrochem. Solid-State Lett.* **2001**, *4*, A49.

(2) (a) Polzot, P.; Laruelle, S.; Grugeon, S.; Dupont, L.; Tarascon, J. M. *Nature* **2000**, *407*, 496. (b) Kwon, C. W.; Campet, G.; Portier, J.; Poquet, A.; Fournès, L.; Labrugère, C.; Jousseaume, B.; Toupance, T.; Choy, J. H.; Subramanian, M. A. *Int. J. Inorg. Mater.* **2001**, *3*, 211.

(3) (a) Kim, J.; Manthiram, A. *Nature* **1997**, *390*, 265. (b) Manthiram, A.; Kim, J. *Chem. Mater.* **1998**, *10*, 2895. (c) Kim, J.; Manthiram, A. *Electrochem. Solid-State Lett.* **1999**, *2*, 55.

(4) (a) Tsang, C.; Kim, J.; Manthiram, A. *J. Solid State Chem.* **1998**, *137*, 28. (b) Jeong, Y. U.; Manthiram, A. *Electrochem. Solid-State Lett.* **1999**, *2*, 421. (c) Jeong, Y. U.; Manthiram, A. *J. Solid State Chem.* **2001**, *156*, 331.

(5) (a) Xu, J. J.; Kinser, A. J.; Owens, B. B.; Smyrl, W. H. *Electrochem. Solid-State Lett.* **1998**, *1*, 1. (b) Leroux, F.; Nazar, L. F. *Solid State Ionics* **1997**, *100*, 103.

(6) Gummow, R. J.; Liles, D. C.; Goodenough, J. B. *Mater. Res. Bull.* **1993**, *28*, 1249.

(7) Hwang, S. J.; Park, H. S.; Choy, J. H.; Campet, G. *Chem. Mater.* **2000**, *12*, 1818.

(8) Kim, J.; Manthiram, A. *J. Electrochem. Soc.* **1997**, *144*, 3077.

(9) (a) Tsang, C.; Dananjay, A.; Kim, J.; Manthiram, A. *Inorg. Chem.* **1996**, *35*, 504. (b) Tsang, C.; Manthiram, A. *J. Mater. Chem.* **1997**, *7*, 1003. (c) Tsang, C.; Lai, S. Y.; Manthiram, A. *Inorg. Chem.* **1997**, *36*, 2206.

(10) Hwang, S. J.; Kwon, C. W.; Portier, J.; Campet, G.; Park, H. S.; Choy, J. H.; Huong, P. V.; Yoshimura, M.; Kakihana, M. *J. Phys. Chem. B* **2002**, *106*, 4053.

(11) Horne, C. R.; Bergmann, U.; Kim, J.; Striebel, K. A.; Manthiram, A.; Cramer, S. P.; Cairns, E. J. *J. Electrochem. Soc.* **2000**, *147*, 395.

(12) (a) Hwang, S. J.; Park, H. S.; Choy, J. H.; Campet, G. *J. Phys. Chem. B* **2000**, *104*, 7612. (b) Park, H. S.; Hwang, S. J.; Choy, J. H. *J. Phys. Chem. B* **2001**, *105*, 4860. (c) Hwang, S. J.; Park, H. S.; Choy, J. H.; Campet, G. *J. Phys. Chem. B* **2001**, *105*, 335.

(13) Choy, J. H.; Hwang, S. J.; Park, N. G. *J. Am. Chem. Soc.* **1997**, *119*, 1624.

(14) Oyanagi, H.; Matsushida, T.; Ito, M.; Kuroda, H. *KEK Rep.* **1984**, *83*, 30.

(15) Thackeray, M. M.; Rossouw, M. H.; de Kock, A.; de la Harpe, A. P.; Gummow, R. J.; Pearce, K.; Liles, D. C. *J. Power Sources* **1993**, *43*−*44*, 289.

(16) Kondrashev, Y. D.; Zaslavsky, A. I. *Izv. Akad. Nauk USSR* **1951**, *15*, 179.

(17) Baur, W. H. *Z. Angew. Phys.* **1970**, *29*, 16.

(18) Porta, P.; Marezio, M.; Remeika, J. P.; Dernier, P. D. *Mater. Res. Bull.* **1972**, *7*, 157.

(19) Battle, P. D.; Gibb, T. C.; Nixon, S.; Harrison, W. T. A. *J. Solid State Chem.* **1988**, *75*, 21.

(20) Stephens, J. S.; Cruickschank, D. W. J. *Acta Crystallogr. B* **1970**, *26*, 222.

(21) The oxygen contents of the nanocrystals prepared under the same reaction conditions were reported to be 1.89 for MnO_2 and 2.03 for CrO_2 (refs 4a and 8).

(22) Hahn, J. E.; Scott, R. A.; Hodgson, K. O.; Doniach, S.; Desjardins, S. R.; Solomon, E. I. *Chem. Phys. Lett.* **1982**, *88*, 595.

(23) Manceau, A.; Gorshkov, A. I.; Drits, V. A. *Am. Miner.* **1992**, *77*, 1133.

(24) Thackeray, M. M. *Prog. Solid State Chem.* **1997**, *25*, 1.

(25) In the course of fitting analysis, the coordination number (CN) was fixed to the crystallographic values while the amplitude reduction factor (S_0^2) was allowed to vary. The best-fit S_0^2 of nanocrystalline MnO_2 is well consistent with that of spinel $LiMn_{1.8}Cr_{0.2}O_4$ within 10% deviation. All of the bond distances (R), Debye−Waller factors (σ^2), and energy shifts (ΔE) were set as variables. However, because of the difficulty in quantitative EXAFS fitting involving distant shells beyond the first one, we have applied several constraints for these variables. First, σ^2 and ΔE were set to be the same for coordination shells within several categories, that is, four (Mn−O) shells at ∼1.90 Å, two (Mn−Mn) shells at 2.85−2.89 Å, and five (Mn−O) shells beyond 3.39 Å. This constraint can be rationalized from the fact that these adjacent shells would possess very similar degree of structural disorder and energy shift. Second, the bond distances in the categories were set to be dependent on each other by using crystallographic data of α-MnO_2 because it is not possible to determine a small path length difference (0.01−0.05 Å) from EXAFS analysis (ref 26).

(26) Meitzner, G. *Microchem. J.* **2002**, *71*, 143.

(27) To estimate the relative concentration of CrO_3 and Cr_2O_3 domains, the amplitude reduction factor (S_0^2) was set as a variable while the coordination number (CN) was fixed to the crystallographic values. All of the bond distances (R), Debye−Waller factors (σ^2), and energy shifts (ΔE) were allowed to vary under the constraint that σ^2 and ΔE are set to be the same for the shells belonging to each domain, that is, three (Cr−O) shells corresponding to CrO_3 domain and two (Cr−O) shells corresponding to Cr_2O_3 domain. Also the (Cr−O) bond distances in each domain were constrained to be dependent on each other by using crystallographic data of CrO_3 and Cr_2O_3, which is due to the limitation in the determination of small path length differences.

(28) Campet, G.; Wen, S. J.; Han, S. D.; Shastry, M. C. R.; Portier, J.; Guizard, C.; Cot, L.; Xu, Y.; Salardennet, J. *Mater. Sci. Eng., B* **1993**, *18*, 201.

(29) Takeda, Y.; Kanno, R.; Tsuji, Y.; Yamamoto, O. *J. Power Sources* **1983**, *9*, 325.